Element Specific Study of Magnetic Anisotropy and Hardening in $SmCo_{5-x}Cu_x$ Thin Films

Georgia Gkouzia,[†] Damian Günzing,[‡] Ruiwen Xie,[†] Teresa Weßels,[¶,‡] Andras Kovacs,[¶] Alpha T. N' Diaye,[§] Márton Major,[†] J. P. Palakkal,[†] Hongbin Zhang,[†] Katharina Ollefs,[‡] Heiko Wende,[‡] and and Lambert Alff[*,†]

†*Department of Materials Science, Technical University of Darmstadt, Darmstadt, Germany*

‡*Faculty of Physics and Center for Nanointegration (CENIDE), University of Duisburg-Essen, Duisburg-Essen, Germany*

¶*Ernst Ruska-Centre for Microscopy and Spectroscopy with Electrons and Peter Grunberg Institute, Forschungszentrum Julich,Julich, Germany*

§*Lawrence Berkeley National Laboratory, Berkeley, USA*

E-mail: georgia.gkouzia@tu-darmstadt.de,ruiwen.xie@tmm.tu-darmstadt.de

Abstract

This work investigates the effect of copper substitution on the magnetic properties of $SmCo_5$ thin films synthesized by molecular beam epitaxy. A series of thin films with varying concentrations of Cu were grown under otherwise identical conditions to disentangle structural and compositional effects on the magnetic behavior. The combined experimental and theoretical results show that Cu substitution at the Co_{3g} cites not only stabilizes the formation of the $SmCo_5$ structure but enhances magnetic anisotropy and coercivity. Density functional theory calculations indicate that $Sm(Co_4Cu_{3g})_5$ possesses a higher single-ion anisotropy as compared to pure $SmCo_5$. In addition, X-ray magnetic circular dichroism reveals that Cu substitution causes an increasing decoupling of Sm $4f$ and Co $3d$ moments. Scanning transmission electron microscopy confirms a homogeneous distribution of elements in a predominantly $SmCo_5$ phase. Our study based on model thin film systems and advanced characterization as well as modelling reveals novel aspects of the complex interplay of intrinsic and extrinsic contributions to magnetic hysteresis in rare earth based magnets.

Keywords

Magnetic films, $SmCo_5$, magnetic hysteresis, ferromagnetic materials

1 Introduction

$SmCo_5$ permanent magnets were already known in the '60s due to their enormously strong uniaxial magnetic anisotropy of about $K_1 = 17.2\,\mathrm{MJ/m^3}$.[1–3] The large magnetocrystalline anisotropy energy (MAE) arises due to the spin-orbit coupling of localized and partially filled $4f$ electrons of Sm and the spin-orbit coupling of the itinerant $3d$ electrons of cobalt in a strong crystal electric field.[4,5] Besides, $SmCo_5$ exhibits a relatively large energy product $(BH)_{\max}$ up to $200\,\mathrm{kJ/m^3}$ and a Curie temperature of 1020 K.

In practical applications, $SmCo_5$-based permanent magnets derive from a more complex

alloy of Sm-Co-Cu-Fe-Zr where after sophisticated heat treatments a unique microstructure emerges.[6,7] The increased demand for high $(BH)_{\max}$ magnets in particular for high-temperature applications in renewable energy technologies has spurred recent interest in the various phenomena leading to high coercivity.[8,9] It is well-known that phase decomposition of the starting alloy results in a cellular microstructure of Sm_2Co_{17} (2:17) with an $SmCo_5$ (1:5) intergranular phase, while a Zr-rich platelet plays a role as pinning site.[10,11] The $SmCo_5$ phase is Cu-rich and the Sm_2Co_{17} phase Fe-rich. Over the years, various studies have investigated the role of the individual elements Cu, Fe, and Zr in intrinsic and extrinsic magnetic properties. However, a complete understanding that could help to overcome the so-called Brown's paradox and help in the development of novel green magnets is still lacking.[12–15]

Sm-Co thin films offer good control over nanostructure and elemental distribution, therefore, providing model structures to understand the specific effects of individual defects on the magnetic properties. Nevertheless, due to the thermodynamic instability of the $SmCo_5$ phase, also in thin films complex decomposition effects do occur. We have recently discovered, a novel phase decomposition regime in molecular beam epitaxy (MBE) grown thin films, resulting in the coexistence of $SmCo_5$ and Sm_2Co_{17} blocks at the nanoscale with a width of only a few nanometers. These films have low coercivity due to their high crystallinity, phase purity, and fully coherent interfaces between $SmCo_5$ and Sm_2Co_{17}.[16] In contrast, sputtered thin films grown at much higher particle energies have a more complex precipitation nanostructure made up of various Sm-rich phases such as $SmCo_3$ and Sm_2Co_7, which can lead to ultra-high coercivity primarily due to pinning at low-symmetry grain boundaries.[17]

Typically different buffer and underlayers made from Ru, Cr, or Cu have been used to ease the growth of Sm-Co thin films. Textured Cr and Ru buffer layers promote the *c*-axis orientation and improve the magnetic properties. Above all, Cu has been widely studied because it not only facilitates the out-of-plane orientation but has been found to have the unique advantage of stabilizing the $CaCu_5$ structure.[18–20] Nevertheless, the magnetic properties of the Sm-Co layer will be affected by diffusion processes from these buffer layers. To address this, we have established a direct growth process on sapphire without any additional underlayer, eliminating the potential impact of diffusing elements. The following results are obtained on a well-controlled series of Cu substituted $SmCo_{1-x}Cu_x$ samples with otherwise mainly identical properties.

2 Methodology

2.1 Experimental part

The base pressure of the used MBE chamber was 10^{-10} mbar. The $SmCo_{5-x}Cu_x$ thin films were deposited by co-evaporation from elemental Sm, Co, and Cu sources. The films were deposited onto *c*-axis oriented Al_2O_3 substrates, known to promote the *c*-axis orientation of the $SmCo_5$ phase. First, a temperature scan was carried out showing that the most favorable temperature for growing a crystalline $SmCo_5$ layer was in this setup 550°C. The substrates were heated from the backside using a diode laser, a technique that avoids contamination from in vacuum heaters. Before evaporation, the substrates were annealed for 1h in the MBE chamber, in order to obtain a clean crystalline substrate surface. For all samples, the deposition rate of the samarium was kept constant at 0.1 Å/sec. The individual deposition rates of cobalt and copper were changed but the sum of the deposition rate (Co plus Cu) was kept constant at 0.1 Å/sec. A series of $SmCo_{5-x}Cu_x$ films was produced with $x = 0.5, 1, 1.5, 2$. The evaporation rates during the growth of the thin films were controlled by using quartz crystal microbalances. The quality of the films was monitored using in-situ reflection high energy electron diffraction (RHEED).

X-ray diffraction (XRD) with Cu K_α radiation on a Rigaku SmartLab system was carried out for the crystallographic and structural

characterization of the films. The thickness of the films was determined to be 30 nm±2 nm. The magnetic properties of the films were measured by a superconducting quantum interface device (SQUID) in two directions, out-of-plane and in-plane of the substrate surface. The coupling of Sm and Co moments has been studied using X-ray magnetic circular dichroism (XMCD) by recording element-specific hysteresis loops. For structural and spectroscopic characterization high-resolution transmission electron microscopy (HR-TEM) was used on cross-sectional specimens prepared along the *c*-axis by focus ion beam milling.

2.2 Computational part

In order to evaluate the single-ion anisotropy of Sm^{3+}, the crystal field parameters (CFPs) were calculated in the frame work of density functional theory (DFT) using the WIEN2k program.[21] The generalized gradient approximation (GGA) form was employed for the exchange correlation functional. The experimental lattice parameters of $SmCo_5$ were adopted for the *ab initio* calculations. Regarding the Cu-doped cases, including $Sm(Co_4Cu_{3g})_5$ and $Sm(Co_4Cu_{2c})_5$, the lattice parameters were fixed to those of $SmCo_5$ considering the relatively small volume change. Therefore, the solely chemical effect of Cu can be explicitly probed. The $RMT \times K_{\max}$ was set to 7 and a $kmeshof9 \times 9 \times 9$ was sampled in the irreducible Brillouin zone. For the calculation of CFPs, we followed the method proposed by Novák *et al.*,[22] in which the local Hamiltonian in the basis of Wannier functions is expanded by a series of spherical tensor operators. In specific, the self-consistent field (SCF) calculation was first performed without spin polarization and with $4f$ electrons in the core. Subsequently, a non-SCF calculation was carried out treating $4f$ as valence states so that the $4f$ states were allowed to hybridize with the transition metal $3d$ states. In addition, we shifted the energy of $3d$ states 0.4 Ry lower to assure appropriate hybridization strength. The Bloch states from the $4f$ energy window were then transformed to Wannier functions using the wien2wannier interface[23] followed by standard Wannierization process by Wannier90.[24]

The obtained CFPs were then used to construct the atomic Hamiltonian of Sm by including also the Coulomb interactions ($\hat{H}_U$), the spin-orbit coupling and the Sm-transition metal exchange coupling ($\hat{H}_{ex}$)

$$\hat{H}_{at} = \hat{H}_U + \lambda \sum_i \hat{s}_i \hat{l}_i + \hat{H}_{CF} + \hat{H}_{ex}. \qquad (1)$$

The eigenvalue of the Hamiltonian was solved using Lanczo's algorithm as implemented in Quanty code.[25] By varying the magnetization direction corresponding to the exchange coupling term, the eigenvalue was then obtained as a function of azimuthal angle.

3 Results and discussion

3.1 Crystal Structure/X-ray diffraction

Figure 1a shows the X-ray diffraction patterns of the $SmCo_{5-x}Cu_x$ films grown onto (001) oriented Al_2O_3 substrates. The main (006) reflection of the substrate appears at 41.67°. The (001)-oriented Al_2O_3 promotes the growth of *c*-axis textured $Sm(Co,Cu)_5$ films, indicated by the presence of (00l)-type reflections. In the film with the lowest Cu content (#1), the main reflection (002) of the $SmCo_5$ phase is observed at 44.218°. Upon increasing the Cu content, the (002) reflection shifts to 45.106° and with an even further increase of Cu content (#4), the reflection shifts again to lower angles (inset Figure 1a). At the same time, the residual reflection of the Sm_2Co_{17} phase decreases and eventually dissappears upon increasing Cu content. The observed non-linear peak shift can be consistently explained as follows: First, the reduction of the 2:17 phase shifts the peak towards the 1:5 peak, as observed previously.[16] Then, the increasing Cu content shifts the peak back, due to the slightly enlarged lattice constant of $SmCu_5$, in agreement with Vegard's law. Note that the phase purity is higher than that of typical sputtered thin films, however, also reflections from a small amount of residual Sm-

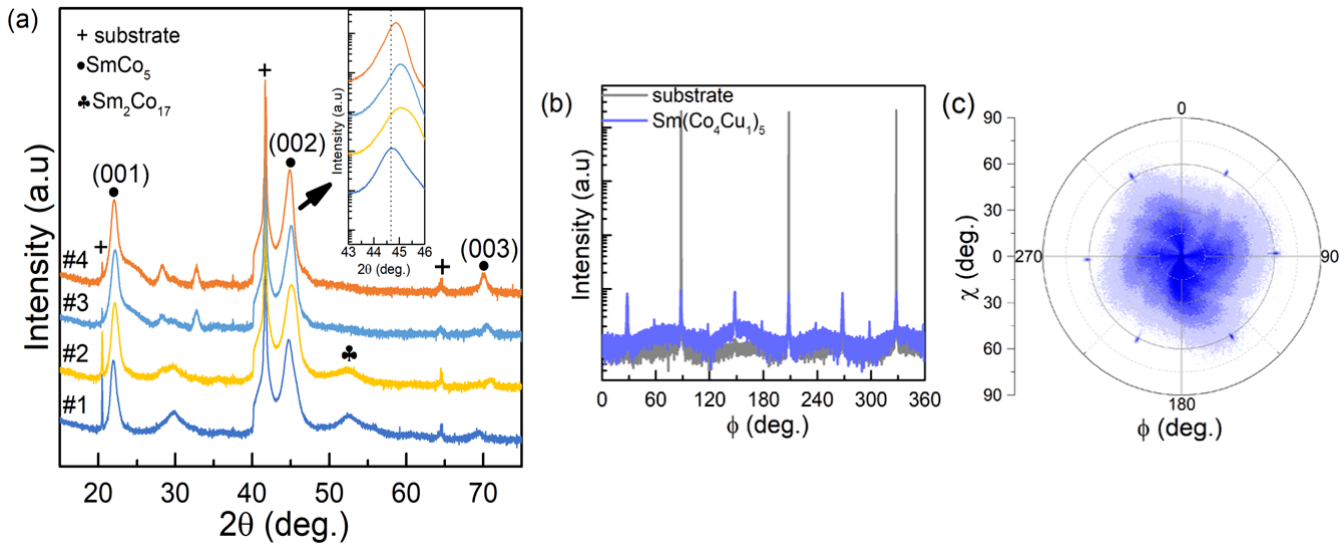

Figure 1: (a) θ-2θ X-ray diffraction patterns of (#1) $SmCo_{4.5}Cu_{0.5}$, (#2) $SmCo_4Cu_1$, (#3) $SmCo_{3.5}Cu_{1.5}$ and (#4) $SmCo_3Cu_2$ thin films grown onto single crystalline Al_2O_3 substrate at 550°C. At 41.67° the 006 reflection of the Al_2O_3 substrate is marked with the plus sign. (b) ϕ scan of the $SmCo_4Cu_1$ film (blue) grown on single crystalline Al_2O_3 substrate (grey) at 550°C.(c) Pole figure of the $SmCo_5$ reflection of the $SmCo_4Cu_1$ film. The reflections confirm the symmetry of the intermetallic phase.

rich phases can still be detected at roughly 29° and 30°. Nevertheless, the overall microstructure remains consistently constant throughout the series.

Azimuth scans have been used to confirm crystal lattice symmetry and epitaxial relations. Here, we show a ϕ-scan of the diffraction peak of the $SmCo_4Cu_1$ sample with respect to the substrate. Figure 1b shows the 104 reflection (grey 2θ=35.03° and x=38.02°) of the substrate which is rhombohedral and the $SmCo_4Cu_1$ sample (blue) which is hexagonal. The ϕ-scan shows three peaks which indicate the thee-fold symmetry of the Al_2O_3 substrate. Six peaks are obtained for the $SmCo_4Cu_1$ film which shows the six-fold symmetry and proves its hexagonal phase. The observed peaks correspond to the 201 reflection of the $SmCo_5$ phase. The pole figure of the 201 reflections, Figure 1c, shows the high-intensity Bragg peaks in blue. The distribution of the reflections indicates a crystalline, highly textured film.

3.2 Magnetization measurements

The magnetic properties of the films were investigated using a superconducting quantum interference device (SQUID) MPMS XL magnetometer by Quantum Design. The measurements have been performed at 300 K with external fields up to 6 Tesla. The diamagnetic contribution from the Al_2O_3 substrate has been subtracted by correcting the slope between 4 and 6 Tesla.

Usually, Cu has been used as doping in $SmCo_5$ thin films grown onto Cr or Ru buffer layers.[26,27] As mentioned above, in this work, no additional underlayers have been used, and the $SmCo_{5-x}Cu_x$ films were deposited directly on top of Al_2O_3 substrates. The hysteresis loops of the out-of-plane direction are shown in Figure 2. The easy axis of magnetization is out of a plane for all samples while the hard axis is in-plane as shown in Figure 4. Starting from the film with the lowest Cu concentration, a remanent magnetization of 0.6 T can be observed and the coercivity reaches 1.08 T. Upon increasing the Cu ratio, the coercivity drastically increases up to 1.64 T whereas the remanent and saturation magnetization, as expected due to Cu dilution of Co moments, are becoming smaller (see Fig. 3). Even further increase of Cu results in a rapid decrease of coercivity

to 1.23 Tesla.

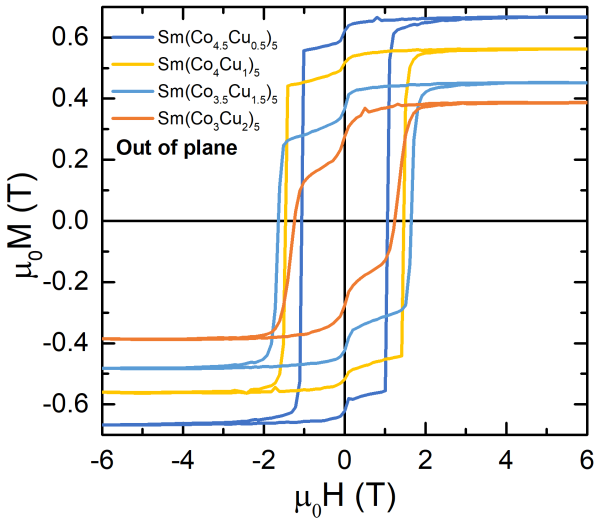

Figure 2: Magnetization curves of the $SmCo_{5-x}Cu_x$ thin films measured in the out-of-plane (OOP) direction as a function of applied field at 300 K.

There are two sites where Cu can substitutes Co, namely Co_{2c} and Co_{3g}.[28] Generally, high levels of Cu substitution either at Co_{2c} or Co_{3g} sites reduce the total exchange energy constant, since Cu blocks the weak Co-Sm $3d$-$5d$ coupling. The impact of Cu doping on Co can be understood by the studies on the YCo_5 system. For YCo_5, doping of Cu at Co_{3g} sites increases the magnetic anisotropy,[29] while doping at $2c$ sites is expected to reduce the magnetic anisotropy due to the larger K_1 value of Co_{2c} compared to Co_{3g}.

As the thin film microstructure is similar in all cases, we assume that also extrinisc contributions to the coercivity are comparable. Therefore, we suggest that the increased coercivity is correlated with an increased intrinsic anisotropy resulting from Cu substitution at the Co_{3g} sites. To corroborate this hypothesis, we discuss DFT based modelling in the next section (Sec. 3.5). In-plane magnetization measurements shown in Figure 4 further support an increased anisotropy for $SmCo_4Cu_1$ and $SmCo_{3.5}Cu_{1.5}$. Another factor leading to increased intrinsic anisotropy, is the improved crystallization of the 1:5 phase due to Cu substitution.[30] Interestingly, in the out-of-plane loops shown in Figure 3, a small kink appears at zero

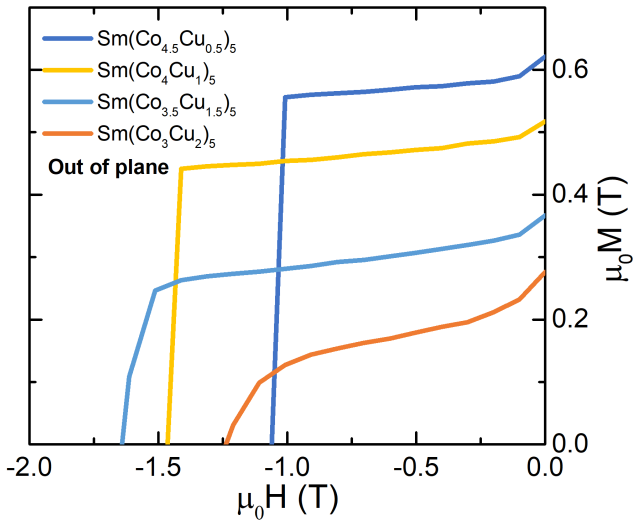

Figure 3: Demagnetization curves of the $SmCo_{5-x}Cu_x$ thin films as a function of applied field at 300 K.

field. This kink could be associated with the presence of a residual soft magnetic nanocrystalline or amorphous phase.

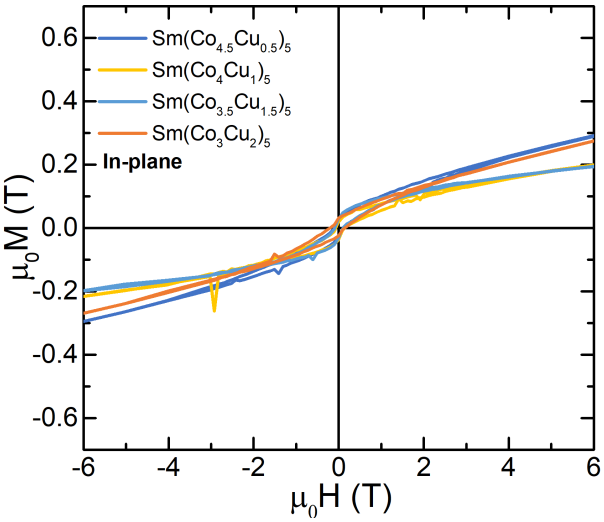

Figure 4: Magnetization curves of the $SmCo_{5-x}Cu_x$ thin films measured in the in-plane (IP) direction as a function of applied field at 300 K.

3.3 X-ray magnetic circular dichroism (XMCD)

X-ray magnetic circular dichroism (XMCD) has been performed at the bending magnet beamline 6.3.1 of the Advanced Light Source

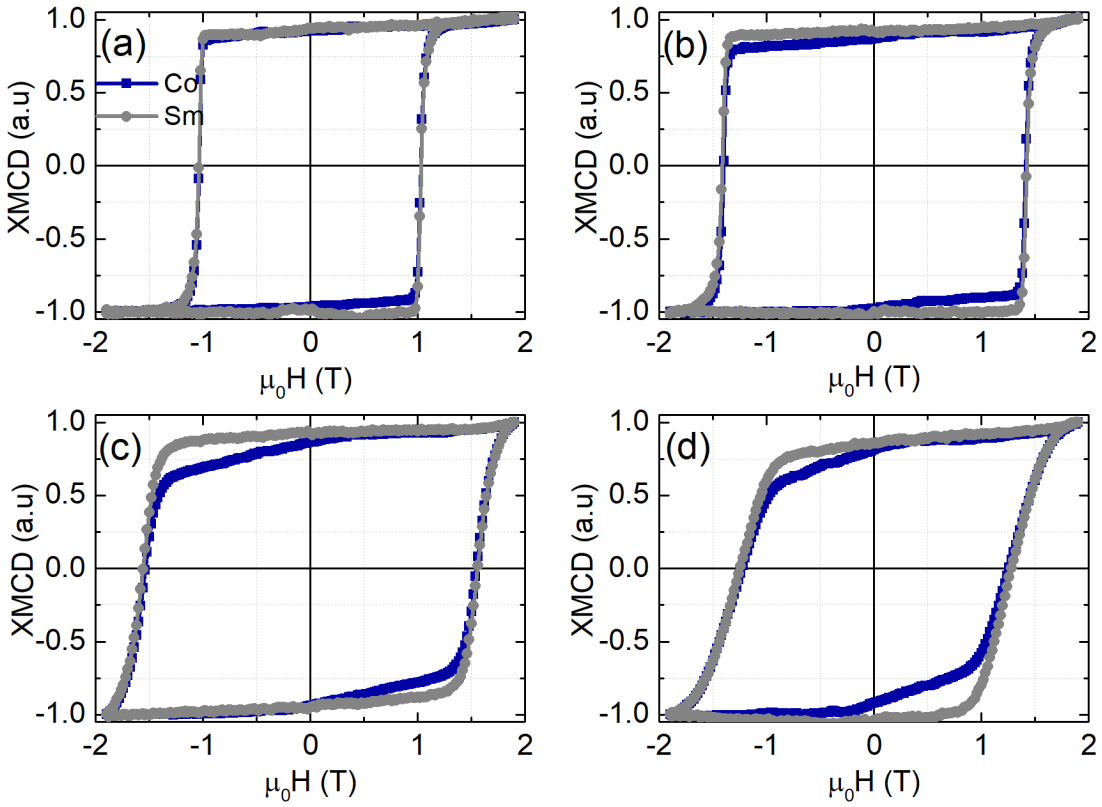

Figure 5: Element specific hysteresis loops for the Sm $M_{4,5}$ (grey) and Co $L_{2,3}$-edges (blue) recorded at room temperature applying positive and negative 1.9 T external fields in out-of-plane direction for the following samples (a) $SmCo_{4.5}Cu_{0.5}$ (b) $SmCo_4Cu_1$ (c) $SmCo_{3.5}Cu_{1.5}$ and (d) $SmCo_3Cu_2$.

(ALS) at Lawrence Berkeley National Laboratory. The XMCD measurements were carried out using external applied magnetic fields of negative and positive 1.9 T with a fixed polarization, at room temperature. As a detection method luminescence yield (LY) was used, which probes the full thickness of the film, due to the luminescence of oxygen in the Al_2O_3 substrate. Simultaneously, the electron current was measured as total electron yield (TEY) detection. Element-specific hysteresis loops have been recorded at fixed energies for Co and Sm. X-ray absorption magnetic measurements for Sm $M_{4,5}$ and Co $L_{2,3}$-edges have been used.

The strength of element-specific hysteresis measurements is the quantitative separation and determination of spin and orbital moments.[31] The samples have been measured in out-of-plane direction shown in Figure 5 which includes the Sm and Co element-specific loops.

The Co and Sm curves lie almost perfectly on top of each other for the $SmCo_{4.5}Cu_{0.5}$ film shown in Figure 5a. This confirms the exchange coupling between the rare earth and the transition metal. Upon increase of Cu substitution, a "gap" between cobalt and samarium appears in the demagnetizing curves, the second quadrant. The data shows that Cu causes a continuous decoupling of Sm and Co moments. Increasing Cu substitution in Co sub-lattice softens the Co moments and decouples them from the Sm moments. The dilution with Cu is also the reason of the reduced total magnetization of the films. In contrast, samarium moments are only softened at higher Cu concentrations, also supported by the reduced critcial temperature of the Cu-rich compounds.

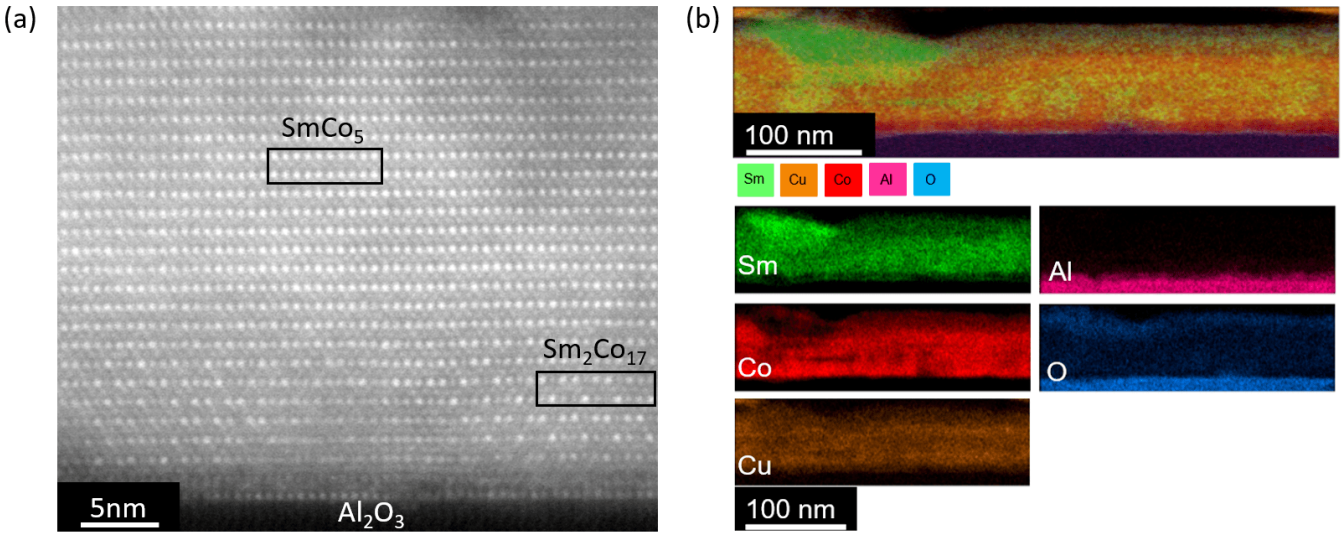

Figure 6: (a)Scanning transmission electron microscopy/high-resolution high-angle annular dark-field (STEM/HAADF) image showing with atomic resolution the interface of the $SmCo_4Cu_1$ thin film to the substrate. (b) EDS of the same film showing the distribution of Sm, Co, Cu, Al, and oxygen.

3.4 Transition electron microscopy

Figure 6a shows a scanning transmission electron microscopy/high-resolution high-angle annular dark-field (STEM/HAADF) image of the $SmCo_4Cu_1$ film confirming the high crystalline quality. Note, that the 2:17 phase seems to be located at the interface to the substrate (in contrast to an intertwined nanostructure as observed in pure 1:5 thin films[16]). The 2:17 phase can be recognized in this FIB cut by its characteristic "dumbbell" structure. Energy dispersive X-ray (EDX) mapping of the $SmCo_4Cu_1$ thin film shows a homogeneous distribution of Sm, Co and Cu, as well as a negligible amount of oxygen across the entire film (see Fig. 6b). Note in particular, that Cu and Co atoms are equally distributed giving no evidence for Cu-rich and Cu-poor regions on this scale. We have chosen an image, where at the surface a Sm-rich grain is formed which will, however, not play a role in the hysteresis behavior, but might be responsible for the zero field kink in the SQUID measurement which is absent in the XMCD measurement. At other positions within the bulk of the 1:5 thin film, no variations of the Sm content could be resolved.

3.5 Discussion

The magnetization curves of the $SmCo_{5-x}Cu_x$ films measured at room temperature were shown in Figure 2. It is clear that Cu substitution affects the coercivity which reaches a maximum value of 1.64 T. The presence of Cu at low concentrations enhances coercivity up to the $SmCo_{3.5}Cu_{1.5}$. Following the X-ray diffraction patterns, the 1:5 phase is by far the predominant phase in all samples. A small fraction of the 2:17 phase which is the result of the natural phase decomposition, is fully suppressed for higher Cu substitution. XMCD element-specific hysteresis loops proved that Cu substitution results in an increasing decoupling of the Sm and Co moments. Last but not least, transition electron microscopy confirmed that the films were dominated by mainly the 1:5 phase.

We first discuss the effect of Cu on the intrinsic magnetic anisotropy of $SmCo_5$, especially the single-ion anisotropy (SIA) of Sm^{3+}. While intuitively one would expect an immediate decrease of intrinsic magnetic anisotropy, using the computational methods described in Sec. 2.2 show a different and more complex behavior. The calculated CFPs B_{lm} for $SmCo_5$, $Sm(Co_4Cu_{3g})_5$ and $Sm(Co_4Cu_{2c})_5$ are listed in Table 1. $SmCo_5$ belongs to the point group D_{6h}

therefore only B_{20}, B_{40}, B_{60} and $B_{6\pm6}$ retain. The evaluated B_{lm} values using the Wannier basic are comparable with measured values. In particular, the magnitude of B_{20} is dominant and determines largely the magnetic anisotropy. In the case of Sm^{3+}, a negative B_{20} indicates uniaxial magnetic anisotropy. With Cu doped on the $3g$ site, B_{20} is more negative, indicating that the SIA of Sm^{3+} is indeed enhanced. In contrast, the Cu doping on the $2c$ site tends to lower the SIA of Sm^{3+}. Note that the number of existing B_{lm} parameters in $Sm(Co_4Cu_{3g})_5$ is larger due to its lower symmetry with point group D_{2h}

Table 1: Crystal field parameters (in units of Kelvin) for $Sm^{3+}Co_5$, $Sm^{3+}(Co_4Cu_{3g})_5$ and $Sm^{3+}(Co_4Cu_{2c})_5$. For comparison, the experimental values are taken from Ref.[32]

B_{lm} (K)	$SmCo_5$	Expt.	$Sm(Co_4Cu_{3g})_5$	$Sm(Co_4Cu_{2c})_5$
B_{20}	-1068	-840	-1380	-867
$B_{2\pm2}$	-	-	168	-
B_{40}	5	200	77	-91
$B_{4\pm2}$	-	-	102	-
$B_{4\pm4}$	-	-	-44	-
B_{60}	-473	0	-472	-430
$B_{6\pm2}$	-	-	-14	-
$B_{6\pm4}$	-	-	-34	-
$B_{6\pm6}$	494	6	501	456

However, another important aspect to be reminded of is the weaker exchange coupling between Sm and its neighboring Co atoms if the non-magnetic Cu is introduced into the system. The exchange field in $SmCo_5$ is set to be 250 T according to previous experimental[33] and theoretical[34] work, while for $Sm(Co_4Cu_{3g})_5$ and $Sm(Co_4Cu_{2c})_5$, the exchange fields are rescaled based on the calculated J_{SmCo} values contributed from the first-nearest neighbors of Sm with respect to the J_{SmCo} of $SmCo_5$. The exchange coupling parameters were calculated using the 'jx' post-processing code in OpenMX[35] under LDA + U regime with U = 6.7 eV and J = 0.7 eV applied on Sm $4f$ states. Accordingly, we set the exchange fields of $Sm(Co_4Cu_{3g})_5$ and $Sm(Co_4Cu_{2c})_5$ to 201 and 230 T, respectively. The Coulomb interaction parameters and the spin-orbit coupling strength are taken from Ref.[36] By varying the exchange field direction which is represented by the azimuthal angle θ, we show in Fig. 7 the eigenvalue E_{ani} of $\hat{H}_{at}$ as a function of θ. It can be explicitly observed that the Sm^{3+} in $Sm(Co_4Cu_{3g})_5$ possesses the highest SIA while in $Sm(Co_4Cu_{2c})_5$ the SIA is the lowest. By fitting the energy curve to

$$E_{ani}(\theta) = K_1\sin^2\theta + K_2\sin^4\theta + K_3\sin^6\theta, \quad (2)$$

we obtain K_1 of 21 meV, 24 meV and 17 meV for $SmCo_5$, $Sm(Co_4Cu_{3g})_5$ and $Sm(Co_4Cu_{2c})_5$, respectively. Note here that we omitted the K_3' term associated with $K_3'\sin^6\theta\cos6\phi$ since we found K_3' is rather small. Besides, the Cu doping effect on the Co side can be approximated using YCo_5 as a prototype. It has been reported that the $3g$ sites doping of Cu increases the magnetic anisotropy of YCo_5[29] while the $2c$ sites doping is expected to reduce the magnetic anisotropy due to larger K_1 of Co_{2c} than that of Co_{3g}. In addition, according to our DFT calculations, the $2c$ sites doping is only energetically favorable by about 7 meV/atom as compared to the $3g$ site doping, which strongly implies a statistically random distribution on both sites in reality. Therefore, concerning the contrasting roles played by Cu with different Wyckoff position occupations, the non-monotonous change of magnetic anisotropy with Cu doping content can be expected, as also observed in Ce-Co based systems.[37,38]

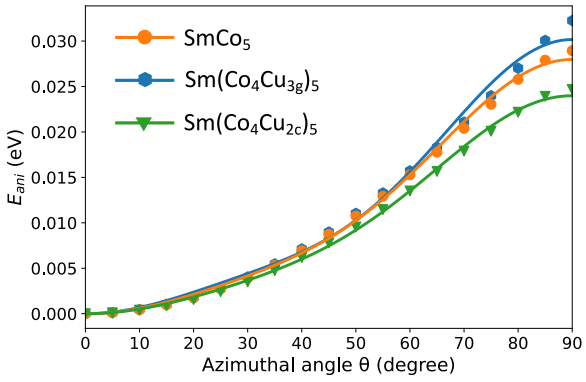

Figure 7: Ground state energy of Sm $4f$ shell in $SmCo_5$ (orange circle), $Sm(Co_4Cu_{3g})_5$ (blue hexagons), $Sm(Co_4Cu_{2c})_5$ (green triangle) as a function of magnetization direction represented by the azimuthal angle θ.

Despite the evaluated non-monotonous dependence of the magnetic anisotropy on the Cu doping concentration, it should be noted that the intrinsic magnetic anisotropy may only play a prominent role at low temperatures. The E_{ani} difference between $Sm(Co_4Cu_{3g})_5$ and $Sm(Co_4Cu_{2c})_5$ is approximately 7 meV, which amounts to a temperature change of 81 K. In this regard, it is a formidable task to directly relate the change of intrinsic magnetic anisotropy to that of the extrinsic coercivity. Nonetheless, it is still intriguing to characterize the intrinsic properties of Cu-doped $SmCo_5$ system so as to help bridging the gap between the microscopic equilibrium properties and the macroscopic coercivity.[39]

From a macroscopic point of view, Sm-rich precipitates as well as the formation of many different Sm-Co phases and structural disorder phenomena are strongly connected to high coercivity values in sputtered Sm-Co films.[17] Sayama *et al.*[40] suggested that the origin of high perpendicular anisotropy in $SmCo_5$ thin films on Cu buffer layers is related to the diffusion of Cu atoms into the $SmCo_5$ structure. Note that this diffusion effect is excluded in the here presented study. Our buffer-free MBE-grown thin films, exhibit a uniform distribution of Sm, Co, and Cu in the bulk of the thin film. The layer of Sm_2Co_17 at the substrate interface and Sm-rich large precipitates will not contribute to a systematic change of the hysteresis itself. As the defect structure is similar throughout the consistent series of thin films, we correlate the increased coercivity to the increased intrinsic magnetocrystalline anisotropy upon Cu substitution.

4 Conclusions

In summary, our investigation of highly crystalline $SmCo_{5-x}Cu_x$ thin films grown by molecular beam epitaxy (MBE) on Al_2O_3 substrates in combination with advanced computational and characterization methods, has revealed that copper substitution enhances the intrinsic magnetic anisotropy, correlated with an increase in coercivity. As the microstructure of the thin films is similar, this DFT theory supported intrinsic anisotropy increase is responsible for the change of the macroscopic demagnetization behavior. The practical applicability of Cu to replace Co is limited of course by the induced overall reduction of the total magnetic moment, acting negatively on the $(BH)_{\max}$ product. X-ray magnetic circular dichroism provided clear evidence of a decoupling of Sm and Co moments in the presence of Cu. TEM in the scanning high-resolution high-angle annular dark-field (STEM/HAADF) mode confirms the high crystalline quality and the absence of a large number of (random) grain boundaries, while EDS on the FIB lamellae shows a homogeneous distribution of all involved elements. Based on thin film model systems, our study provides novel insight in the complex hardening mechanisms in rare earth based permanent magnetic materials by disentangling different sources of intrinsic and extrinsic contributions to the hysteresis behavior.

Acknowledgement We acknowledge the financial support from the German Research Foundation (DFG) in the framework of the CRC/TRR 270 (Project No. 405553726), projects A02, A03, A05, B05, and Z01/02.

Supporting Information Available

A listing of the contents of each file supplied as Supporting Information should be included. For instructions on what should be included in the Supporting Information as well as how to prepare this material for publications, refer to the journal's Instructions for Authors.

The following files are available free of charge.

- Filename: brief description
- Filename: brief description

References

(1) Coey, J. M. *Magnetism and magnetic materials*; Cambridge university press, 2010.

(2) Strnat, K.; Hoffer, G.; Olson, J.; Ostertag, W.; Becker, J. A family of new cobalt-base permanent magnet materials. *Journal of Applied Physics* **1967**, *38*, 1001–1002.

(3) Strnat, K. Rare earth-cobalt permanent magnets. *Handbook of Ferromagnetic Materials* **1988**, *4*, 131–209.

(4) Larson, P.; Mazin, I. Magnetic properties of SmCo 5 and YCo 5. *Journal of applied physics* **2003**, *93*, 6888–6890.

(5) Ucar, H.; Choudhary, R.; Paudyal, D. An overview of the first principles studies of doped RE-TM5 systems for the development of hard magnetic properties. *Journal of Magnetism and Magnetic Materials* **2020**, *496*, 165902.

(6) Mishra, R. K.; Thomas, G.; Yoneyama, T.; Fukuno, A.; Ojima, T. Microstructure and properties of step aged rare earth alloy magnets. *Journal of Applied Physics* **1981**, *52*, 2517–2519.

(7) Sepehri-Amin, H.; Thielsch, J.; Fischbacher, J.; Ohkubo, T.; Schrefl, T.; Gutfleisch, O.; Hono, K. Correlation of microchemistry of cell boundary phase and interface structure to the coercivity of Sm (Co0. 784Fe0. 100Cu0. 088Zr0. 028) 7.19 sintered magnets. *Acta Materialia* **2017**, *126*, 1–10.

(8) Gutfleisch, O.; Willard, M. A.; Brück, E.; Chen, C. H.; Sankar, S.; Liu, J. P. Magnetic materials and devices for the 21st century: stronger, lighter, and more energy efficient. *Advanced materials* **2011**, *23*, 821–842.

(9) Gutfleisch, O. High-temperature samarium cobalt permanent magnets. *Nanoscale magnetic materials and applications* **2009**, 337–372.

(10) Maury, C.; Rabenberg, L.; Allibert, C. Genesis of the cell microstructure in the Sm (Co, Fe, Cu, Zr) permanent magnets with 2: 17 type. *physica status solidi (a)* **1993**, *140*, 57–72.

(11) Duerrschnabel, M.; Yi, M.; Uestuener, K.; Liesegang, M.; Katter, M.; Kleebe, H.-J.; Xu, B.; Gutfleisch, O.; Molina-Luna, L. Atomic structure and domain wall pinning in samarium-cobalt-based permanent magnets. *Nature communications* **2017**, *8*, 1–7.

(12) Hadjipanayis, G.; Tang, W.; Zhang, Y.; Chui, S.; Liu, J.; Chen, C.; Kronmuller, H. High temperature 2: 17 magnets: relationship of magnetic properties to microstructure and processing. *IEEE transactions on magnetics* **2000**, *36*, 3382–3387.

(13) Xiong, X. Y.; Ohkubo, T.; Koyama, T.; Ohashi, K.; Tawara, Y.; Hono, K. The microstructure of sintered Sm (Co0. 72Fe0. 20Cu0. 055Zr0. 025) 7.5 permanent magnet studied by atom probe. *Acta Materialia* **2004**, *52*, 737–748.

(14) Wu, S.; Zhang, D.-T.; Yue, M.; Wang, Y.-Q.; Shang, Z.-F.; Wu, D.; Liang, J.-M. In-situ observation of magnetization reversal process of Sm (Co, Cu, Fe, Zr) z magnets with different Fe contents. *Rare Metals* **2020**, *39*, 250–255.

(15) Shang, Z.; Yue, M.; Li, Y.; Zhang, D.; Xie, Z.; Wang, Y. The effect of multiscale Cu distribution regulation on magnetic properties of Sm (CoFeCuZr) z magnets. *Journal of Magnetism and Magnetic Materials* **2020**, *502*, 166484.

(16) Sharma, S.; Zintler, A.; Gunzing, D.; Lill, J.; Meira, D. M.; Eilhardt, R.; Singh, H. K.; Xie, R.; Gkouzia, G.; Major, M., et al. Epitaxy Induced Highly Ordered Sm2Co17–SmCo5 Nanoscale Thin-Film Magnets. *ACS Applied Materials & Interfaces* **2021**, *13*, 32415–32423.

(17) Akdogan, O.; Sepehri-Amin, H.; Dempsey, N.; Ohkubo, T.; Hono, K.; Gutfleisch, O.; Schrefl, T.; Givord, D.

Preparation, characterization, and modeling of ultrahigh coercivity Sm–Co thin films. *Advanced Electronic Materials* **2015**, *1*, 1500009.

(18) Seifert, M.; Neu, V.; Schultz, L. Epitaxial SmCo 5 thin films with perpendicular anisotropy. *Applied Physics Letters* **2009**, *94*, 022501.

(19) Hofer, F. Physical metallurgy and magnetic measurements of SmCo 5-SmCu 5 alloys. *IEEE Transactions on Magnetics* **1970**, *6*, 221–224.

(20) Zhang, W.-y.; Zhang, X.-d.; Yang, Y.-c.; Shen, B.-g. Effect of Cu substitution on structure and magnetic properties of anisotropic SmCo ribbons. *Journal of alloys and compounds* **2003**, *353*, 274–277.

(21) Blaha, P.; Schwarz, K.; Tran, F.; Laskowski, R.; Madsen, G. K.; Marks, L. D. WIEN2k: An APW+ lo program for calculating the properties of solids. *The Journal of chemical physics* **2020**, *152*, 074101.

(22) Novák, P.; Knížek, K.; Kuneš, J. Crystal field parameters with Wannier functions: Application to rare-earth aluminates. *Physical Review B* **2013**, *87*, 205139.

(23) Kuneš, J.; Arita, R.; Wissgott, P.; Toschi, A.; Ikeda, H.; Held, K. Wien2wannier: From linearized augmented plane waves to maximally localized Wannier functions. *Computer Physics Communications* **2010**, *181*, 1888–1895.

(24) Mostofi, A. A.; Yates, J. R.; Lee, Y.-S.; Souza, I.; Vanderbilt, D.; Marzari, N. wannier90: A tool for obtaining maximally-localised Wannier functions. *Computer physics communications* **2008**, *178*, 685–699.

(25) Lu, Y.; Höppner, M.; Gunnarsson, O.; Haverkort, M. Efficient real-frequency solver for dynamical mean-field theory. *Physical Review B* **2014**, *90*, 085102.

(26) Yin, S.; Wang, H.; Zhao, H.; Jiang, Y.; Wang, J. The effects of Cu doping on crystalline structure and magnetic properties of SmCo5-xCux thin films grown on Ru (0002). *Journal of Applied Physics* **2013**, *114*, 213908.

(27) Cui, W.; Ma, L.; Sepehri-Amin, H.; Takahashi, Y.; Hono, K. The influence of grain morphology and easy axis orientation on the coercivity of Sm (Co0. 9Cu0. 1) 5 thin films. *Acta Materialia* **2016**, *107*, 49–58.

(28) Haider, S. K.; Ngo, H. M.; Kim, D.; Kang, Y. S. Enhancement of anisotropy energy of SmCo5 by ceasing the coupling at 2c sites in the crystal lattice with Cu substitution. *Scientific reports* **2021**, *11*, 1–10.

(29) Okumura, H.; Fukushima, T.; Akai, H.; Ogura, M. First-principles Calculation of Magnetocrystalline Anisotropy of Y (Co, Fe, Ni, Cu) _5 Based on Full-potential KKR Green's Function Method. *arXiv preprint arXiv:2204.07384* **2022**,

(30) Ohtake, M.; Nukaga, Y.; Kirino, F.; Futamoto, M. Effects of substrate temperature and Cu underlayer thickness on the formation of SmCo 5 (0001) epitaxial thin films. *Journal of Applied Physics* **2010**, *107*, 09A706.

(31) Stöhr, J. Exploring the microscopic origin of magnetic anisotropies with X-ray magnetic circular dichroism (XMCD) spectroscopy. *Journal of Magnetism and Magnetic Materials* **1999**, *200*, 470–497.

(32) Sankar, S.; Rao, V.; Segal, E.; Wallace, W.; Frederick, W.; Garrett, H. Magnetocrystalline anisotropy of Sm Co 5 and its interpretation on a crystal-field model. *Physical Review B* **1975**, *11*, 435.

(33) Tils, P.; Loewenhaupt, M.; Buschow, K.; Eccleston, R. Crystal and exchange fields in SmCo5 studied by inelastic neutron

scattering. *Journal of alloys and compounds* **1999**, *289*, 28–31.

(34) Patrick, C. E.; Staunton, J. B. Temperature-dependent magnetocrystalline anisotropy of rare earth/transition metal permanent magnets from first principles: the light R Co 5 (R= Y, La-Gd) intermetallics. *Physical Review Materials* **2019**, *3*, 101401.

(35) Terasawa, A.; Matsumoto, M.; Ozaki, T.; Gohda, Y. Efficient algorithm based on liechtenstein method for computing exchange coupling constants using localized basis set. *Journal of the Physical Society of Japan* **2019**, *88*, 114706.

(36) Tripathi, S. XMCD investigation at M4, 5 edges of the rare earth elements in high-performance permanent magnet. **2018**,

(37) Lamichhane, T. N.; Onyszczak, M. T.; Palasyuk, O.; Sharikadze, S.; Kim, T.-H.; Lin, Q.; Kramer, M. J.; McCallum, R.; Wysocki, A. L.; Nguyen, M. C., et al. Single-Crystal Permanent Magnets: Extraordinary Magnetic Behavior in the Ta-, Cu-, and Fe-Substituted Ce Co 5 Systems. *Physical Review Applied* **2019**, *11*, 014052.

(38) Xie, R.; Zhang, H. Mixed valence nature of the Ce 4 f state in CeCo 5 based on spin-polarized DFT+ DMFT calculations. *Physical Review B* **2022**, *106*, 224411.

(39) Matsumoto, M. Magnetism trends in doped Ce-Cu intermetallics in the vicinity of quantum criticality: Realistic Kondo lattice models based on dynamical mean-field theory. *Physical Review Materials* **2020**, *4*, 054401.

(40) Sayama, J.; Mizutani, K.; Asahi, T.; Ariake, J.; Ouchi, K.; Osaka, T. Origin of perpendicular magnetic anisotropy of SmCo5 thin films with Cu underlayer. *Journal of magnetism and magnetic materials* **2006**, *301*, 271–278.

TOC Graphic

Some journals require a graphical entry for the Table of Contents. This should be laid out "print ready" so that the sizing of the text is correct.
Inside the `tocentry` environment, the font used is Helvetica 8 pt, as required by *Journal of the American Chemical Society*.
The surrounding frame is 9 cm by 3.5 cm, which is the maximum permitted for *Journal of the American Chemical Society* graphical table of content entries. The box will not resize if the content is too big: instead it will overflow the edge of the box.
This box and the associated title will always be printed on a separate page at the end of the document.